Darcy's Law-Based Models for Liquid Absorption in Polymer Wicks

Reza Masoodi and Krishna M. Pillai
Dept. of Mechanical Engineering, University of Wisconsin-Milwaukee, Milwaukee, WI 53211

Padma Prabodh Varanasi
S.C. Johnson and Son, Inc., Racine, WI 53403

DOI 10.1002/aic.11322
Published online September 25, 2007 in Wiley InterScience (www.interscience.wiley.com).

Wicking of liquids in polymer wicks made of sintered polymer beads is studied experimentally where three different polymer wicks (made from polycarbonate, polyethylene, and polypropylene) and three different well-characterized liquids (hexadecane, decane, and dodecane) are used to plot the mass of wicked liquid as a function of time. The experimental results are compared with the predictions from the Washburn equation as well as a Darcy's law-based formulation. The suction pressure needed to pull the liquid up a wick in the formulation is modeled using a new energy balance (EB) method and a capillary method. In the former, the released surface energy during wetting is equated to the viscous losses during liquid motion; in the latter, the suction pressure is obtained by treating the wick pore-space as a bundle of capillary tubes. The Darcy's law-based formulation also considers the effect of gravity in its predictions. The newly proposed EB method in conjunction with gravity yields the most satisfying predictions. All parameters used in the proposed model were measured independently and no fitting parameters were used. The success of this method is especially notable for a large-pore polypropylene wick where it was the only model to predict the final steady-state height for the liquid column. © 2007 American Institute of Chemical Engineers *AIChE J,* 53: 2769–2782, 2007

Keywords: capillary model, absorption, wicking, suction pressure, Washburn equation, wick, Darcy's law

Introduction

Wicking is the spontaneous transport of liquid into a porous medium through capillary suction. The capillary suction force arises as a result of the wetting of solid matrix by the invading liquid. Previous research on wicking can be divided into three groups: Study of the relation between the wicking rate and wicking time, study of the relation between the wicking rate and the porous medium characteristics, and study of the wettability of a liquid in terms of the contact angle.

The relation between wicking rate and time was studied by Lucas,[1] Washburn,[2] and Poiseuille.[3] They concluded that the relation between the wicking rate and the square root of time is linear, i.e. $L = k_0 t^m$ in which $m = 0.5$ and L is wicked mass or height. Some researchers[4] tried to find the exact value of m experimentally, where they estimated it to be between 0.46 and 0.48.

In the first few attempts to model the wicking of a liquid into a porous medium, the porous structure was treated as a bundle of capillary tubes, and the inertial and gravitational forces were neglected in the liquid motion modeling. These

Correspondence concerning this article should be addressed to K. M. Pillai at krishna@uwm.edu.

assumptions resulted in the simple Washburn equation for predicting of the wicking rate. Szekely et al.[5] took inertial and gravity forces into account and developed a differential equation for the wicking rate. Unfortunately, the resulting equation is a nonlinear, second order, ordinary differential equation that cannot be solved analytically. In the most wicking applications, the Washburn equation is used when the inertial and gravitational energies can be neglected.

Study of the wicking rate relationship with the porous medium characteristics, especially the fiber orientation, was also a major direction of previous investigations. Chwastiak,[6] Scher,[7] and Hodgson and Berg[8] studied the wicking rate along fibers. The wicking rate across the fibers was also studied by Fowkes,[9] Williams et al.,[10] and Pillai and Advani.[11]

Wetting is an initial requirement for wicking. The parameter indicating wettability is the contact angle, which is the angle between the tangent lines of the liquid–air and solid–liquid interfaces at the solid–air–liquid contact line. The first notable work on wetting was done by Young[12] and Gauss.[13] They tried to find a mathematical equation for contact angle and concluded that the contact angle is a function of surface energies. Dussan and Davis[14] and Dussan[15] reviewed all previous works on the fields of dynamic and static contact angle. In recent years, You-Lo-Hsieh[16] studied liquid wetting and analyzed its relation to fiber morphology and chemistry. Although several researchers tried to find a theoretical equation to predict the magnitude of contact angle, it is still a poorly understood problem.

Wicking tests are used to evaluate the absorption efficiency and liquid transport in the porous materials.[17,18] It is a function of porous media, time, and wettability (in terms of contact angle). Kissa[19] classified the important previous works on the wetting and wicking. Miller[20] experimentally investigated the effect of gravity on upward wicking. Russel and Mao[21] proposed an apparatus and a method to investigate the in-plane anisotropic liquid absorption in nonwoven fabrics. Jeong[22] investigated the slip boundary condition on a porous wall using Stokes approximation. Mao and Russel[23] proposed a theoretical approach to predict the liquid absorption in homogeneous 3D nonwoven structures. They also presented a theoretical analysis of fluid flow in a 2D nonwoven structure by using Darcy's law.[24] Lockington and Parlange[25] presented a new approach to predict water absorption in porous materials based on sorptivity. Gane et al.[26] numerically and experimentally studied the absorption rate and volume dependency on the complexity of porous networks.

As one can see, a majority of the above-mentioned research works is about fibrous materials or textiles where ways of predicting the liquid absorption or wicking into the materials by using the Darcy's law was attempted. The research focused on defining the porous media characteristics, such as the permeability, or the solid–liquid interaction (dynamic contact angle) to use the Darcy's law.

Nowadays, commercial wicks, made by sintering polymer beads, are used by consumer product companies to dispense volatile substances such as room fresheners or insect repellents into the air. For these polymer wicks, which have several important commercial applications, no significant research on their wicking characteristics has been reported. In this article, we used the Darcy's law to predict the liquid absorption in such wicks. We have developed a new expression for the suction pressure in polymer wicks which in conjunction with the Darcy's law compares very well with the experimental results and is found to be superior to the conventional modeling approaches such as the Washburn equation.

Mathematical Theory

We studied the wicking of liquid through a few available commercial wicks to investigate the efficiency of the wicking models. In this regard, we used the following approaches.

Washburn equation

The modified Washburn equation can be used to predict the rise of the liquid front h_f as a function of time t; for our wicking tests it can be expressed as

$$h_f = \left(\frac{R_h \gamma \cos(\theta)}{2\tau^2 \mu}\right)^{1/2} \sqrt{t} \tag{1}$$

where R_h is hydraulic radius, γ is the surface energy or surface tension of the liquid, θ is the contact angle, μ is the viscosity of liquid, and τ is the tortuosity of the porous wick obtained from

$$\tau = \left(\frac{L_e}{L}\right)^2 \tag{2}$$

where L_e is the length of the shortest fluid path through pores between two different points in the wick; L is the length of a straight line path between these two points (see Figure 1).

We used the definition of hydraulic radius, which is the ratio of the fluid volume filled in pores to the wetted surface area of pores, to find the hydraulic radius R_h as

$$R_h = \frac{\varepsilon \pi R_w^2 h}{N \pi d_p h} \tag{3}$$

where R_w is wick radius, d_p is mean pore diameter, h is height of the liquid within the wick, ε is porosity, and N is the number of longitudinal capillaries passing through the wick. We also have the following equation for pores which is obtained by equating the pore volume in the wick with the total volume of the cylindrical tubes inside the wick:

$$\frac{N \pi d_p^2 h}{4} = \varepsilon \pi R_w^2 h \tag{4}$$

After using Eq. 4 in Eq. 3, we have

$$R_h = \frac{R_p}{2} \tag{5}$$

Applying the Eq. 5 result in Eq. 1 gives the final form of Washburn equation as

$$h_f = \left(\frac{R_p \gamma \cos(\theta)}{4\tau^2 \mu}\right)^{1/2} \sqrt{t} \tag{6}$$

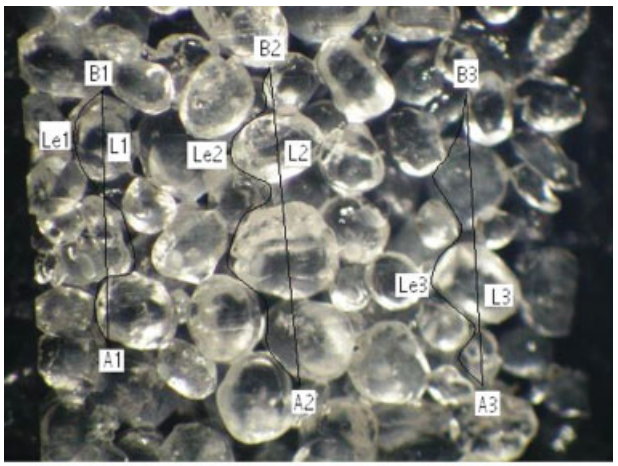

(a)

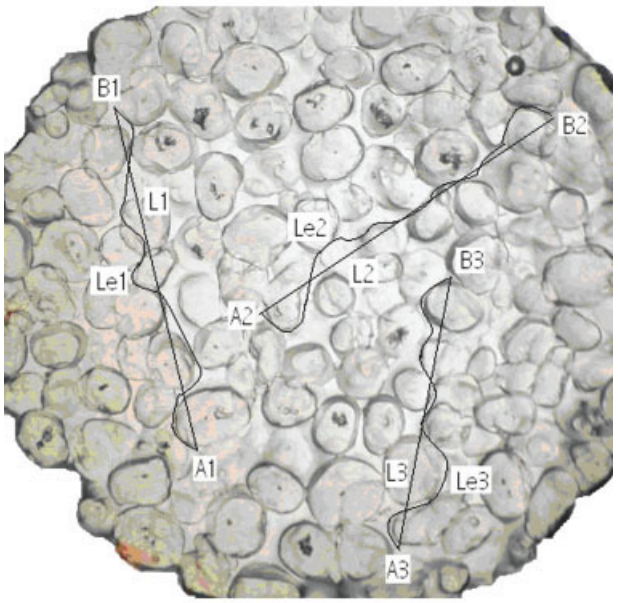

(b)

Figure 1. A typical micrograph of wick C (PP) and the visual description of a method used for measuring tortosity ($\tau = (L_e/L)^2$).

(a) Section along the wick axis; (b) section across the wick axis. [Color figure can be viewed in the online issue, which is available at www.interscience.wiley.com.]

Darcy's law-based wicking formulation

The flow of a liquid in an isotropic porous medium under isothermal conditions is governed by

$$\text{Darcy's Law} : \widetilde{V} = -\frac{K}{\mu}\widetilde{\nabla}P \tag{7}$$

and

$$\text{Equation of Continuity} : \widetilde{\nabla}\cdot\widetilde{V} = 0 \tag{8}$$

where $\widetilde{V}$ is volume averaged liquid velocity and P is the pore averaged modified pressure. ($\widetilde{V}$ and P are obtained after integrating the point-wise liquid velocity and pressure in an averaging volume several times bigger than the particles of a porous medium.[27,28])

The modified pressure P is defined in such a way so as to include the effects of gravity-induced liquid motion in a porous medium and is combined with the pore averaged hydrodynamic pressure p as

$$P = p + \rho g h \tag{9}$$

where h is the height of a point within a fully saturated (or fully wetted) porous medium. We would now model the motion of a liquid within a porous polymer wick as shown in Figure 2. The upward wicking of liquid in the vertical wick is characterized by a clearly defined and upwardly mobile liquid front. It is common to assume that the wick below the rising front is fully wet, i.e., all the pore spaces in the porous wick are occupied by the liquid after it has displaced air. As a result, motion of liquid behind the rising front in the wet wick is governed by Eqs. 7 and 8. For the one-dimensional fluid motion described in Figure 2, the Darcy's law and continuity equation reduce to

$$V = -\frac{K}{\mu}\frac{dP}{dh} \tag{10}$$

and

$$\frac{dV}{dh} = 0 \tag{11}$$

The pressure distribution in the wetted wick is given by

$$\frac{d^2P}{dh^2} = 0 \tag{12}$$

which is obtained by combining Eqs. 10 and 11, and noting that K and μ are constants. Integration of Eq. 12 results into a general solution of the form $P(h) = Ah + B$ where the constants A and B are evaluated using the boundary conditions

$$p = p_{\text{atm}} \; at \; h = 0 \tag{13a}$$

and

$$p = p_{\text{atm}} - p_s \text{ at } h = h_f \tag{13b}$$

that are in terms of the pore averaged hydrodynamic pressure p. Note that p_s is the suction pressure created at the liquid front due to the capillary action. Equations 13a and 13b can be transformed in terms of the modified pressure P as

$$P = p_{\text{atm}} \text{ at } h = 0 \tag{14a}$$

$$P = (p_{\text{atm}} - p_s) + \rho g h_f \text{ at } h = h_f \tag{14b}$$

Use of the boundary conditions (14a) and (14b) with the general solution of Eq. 12 results into the following expression for the modified pressure:

$$P(h) = p_{\text{atm}} + \rho g h - p_s\frac{h}{h_f} \tag{15}$$

(a)

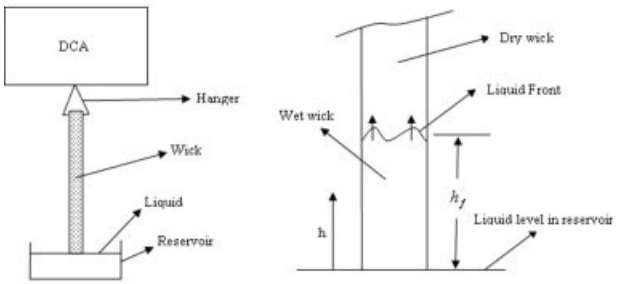

(b)

Figure 2. A photo and schematic of the real setup developed using DCA for the wicking and contact angle tests.

[Color figure can be viewed in the online issue, which is available at www.interscience.wiley.com.]

Note that this solution is valid for $0 \leq h \leq h_f(t)$ where the front height h_f is a function of time. An expression for h_f can be derived by relating front speed $\frac{dh_f}{dt}$ with the Darcy velocity (Eq. 10) at front h_f as

$$\frac{dh_f}{dt} = \frac{V(h = h_f)}{\varepsilon} = -\frac{K}{\varepsilon\mu}\frac{dP}{dh} \tag{16}$$

which through the use of Eq. 15 results in

$$\frac{dh_f}{dt} = \frac{K}{\varepsilon\mu}\left(\frac{p_s}{h_f} - \rho g\right) \tag{17}$$

After separation of variables and integration with the initial value of $h_f(t = 0) = 0$, we have

$$p_s \ln\left|\frac{p_s}{p_s - \rho g h_f}\right| - \rho g h_f = \frac{\rho^2 g^2 K}{\varepsilon\mu} t \tag{18}$$

which is an implicit equation for the liquid-front height h_f in the wick.

Neglecting the Gravity Effects. We can neglect the effect of gravity for wicking in smaller samples. After neglecting the gravity term, integration of Eq. 17 gives us

$$h_f = \sqrt{\frac{2Kp_s}{\varepsilon\ \mu} t} \tag{19}$$

The rise of a liquid in a wick leads to rise in the mass of the wick. The plot of the wicked liquid mass versus time has been used to study and characterize wicking in the past. So note that the mass of fluid absorbed by the wick can be related to h_f through

$$m = \varepsilon\ \rho\ \pi\ R_w^2\ h_f \tag{20}$$

On studying Eqs. 18 and 19 for h_f, we note that suction pressure p_s is an important parameter for predicting the evolution of h_f with time. We will now present two different ways of estimating the suction pressure p_s.

Capillary Model. Here the porous wick is assumed to be a bundle of vertically aligned capillary tubes, and the suction pressure is considered to be the capillary pressure. Based on the Laplace equation, the capillary pressure in a cylindrical tube is given by

$$p_c = \frac{2\gamma\cos(\theta)}{R_p} \tag{21}$$

Replacing of suction pressure in Eq. 18 with capillary pressure (i.e., $p_s = p_c$) leads to

$$p_c \ln\left|\frac{p_c}{p_c - \rho g h_f}\right| - \rho g h_f = \frac{\rho^2 g^2 K}{\varepsilon\mu} t \tag{22}$$

We obtain the final form of the liquid-front height (or the liquid-column height) in the wick for the case of neglecting the gravity effects after using the capillary pressure in a cylindrical tube, Eq. 21, as the suction pressure in Eq. 19:

$$h_f = \sqrt{\frac{4K\gamma\cos(\theta)}{\varepsilon\mu R_p}}\sqrt{t} \tag{23}$$

Energy Balance Model. Here, to find an alternative expression for the suction pressure, we apply the energy balance (EB) principle to wicking. The amount of energy needed to raise the liquid in the wick is equal to the sum of the viscous energy dissipated by the fluid, the energy spent on accelerating the fluid from zero to the wicking speed, and the energy needed to overcome the gravity. The inertial

energy can be neglected in these kinds of experiments as speed of the liquid is very small. We neglect the gravity effects at this stage as well, though we include it elsewhere through the Darcy's law and the modified pressure (Eqs. 9 and 10). So we balanced the reduction of free surface energy when a liquid moves within a wick with the viscose dissipation energy. As the liquid moves through a porous medium, it reduces the dry solid–air interface area and thus increases the wetted solid–liquid interface area. If γ_s stands for the surface energy of the dry surface (or the solid–air interface), and γ_{sl} stands for surface energy of the wetted surface areas (or the solid–liquid interface), then EB leads to

$$(\gamma_s - \gamma_{sl})\, dA = -dw_v \tag{24}$$

in which dA is the interfacial area and w_v is viscous work done by the flow of the liquid. According to Young's equation,[12] the relation between the contact angle and surface energy is given by

$$\cos\theta = \frac{\gamma_s - \gamma_{sl}}{\gamma} \tag{25}$$

Based on Eq. 25, the term $(\gamma_s - \gamma_{sl})$ in Eq. 24 can be replaced by $\gamma \cos\theta$. So we have

$$-dw_v = \gamma \cos\theta\, dA \tag{26}$$

Based on our initial investigation of pore structure by study the wick micrographs (Figure 1), we proposed that the porous wick be composed of spherical beads. The number of beads with radii between r and $(r + dr)$ is given by $dM(r) = M\phi(r)dr$ where M is the total number of the beads in the wick and ϕ is the probability density function. Hence, the total volume of beads is

$$V_b = \int_0^\infty \frac{4}{3}\pi r^2 dM(r) = \frac{4}{3}\pi M M_3 \text{ where } M_3 = \int_0^\infty r^3\phi(r)dr \tag{27}$$

If V_t is the total volume of the wick, then the wick porosity can be estimated as

$$\varepsilon = 1 - \frac{V_b}{V_t} = 1 - \frac{4\pi M M_3}{3A_{cs}L_w} \tag{28}$$

Similarly dA, the increase in the wetted surface area within the cylindrical wick as the liquid moves up by dh_f, is given by

$$dA = \int_0^\infty 4\pi r^2 dM(r)\left(\frac{dh_f}{L_w}\right) = 4\pi M M_2\left(\frac{dh_f}{L_w}\right) \text{ where } M_2 = \int_0^\infty r^2\phi(r)dr \tag{29}$$

On replacing M in Eq. 29 with its equivalent expression from Eq. 28, we get

$$dA = 3A_{cs}(1-\varepsilon)\frac{M_2}{M_3}dh_f \tag{30}$$

which allows the change in the wet interface area to be expressed in terms of the change in the liquid-column height. Substitution of dA from Eq. 30 into Eq. 26 gives the final form for the increment in dissipation energy as

$$dw_v = -\frac{3A_{cs}(1-\varepsilon)\gamma\cos(\theta)}{R_e}dh_f \tag{31}$$

where effective radius R_e is defined as $R_e = \frac{M_3}{M_2}$. The mechanical work needed to move the fluid by dh_f is $dw_m = F_p dh_f$ where F_p is the pulling force that "pulls" the liquid front through the pores of the wick. As per the definition of suction pressure, this pulling force should be equal to $p_s.\varepsilon.A_{cs}$. As a result

$$dw_m = \varepsilon.p_s A_{cs} dh_f \tag{32}$$

According to the EB principle, the total energy of system after moving the front liquid into the wick should be equal to its initial value which was zero. So the summation of the left sides of Eqs. 31 and 32 should be zero, i.e., $dw_v + dw_m = 0$, which results in an expression for suction pressure as

$$p_s = \frac{3(1-\varepsilon)\gamma\cos(\theta)}{\varepsilon R_e} \tag{33}$$

Note that if all beads have the same radius of R_b in a simplified ideal case, then $R_e = R_b$ and we have

$$p_s = \frac{3(1-\varepsilon)\gamma\cos(\theta)}{\varepsilon R_b} \tag{34}$$

We have made the following two assumptions in obtaining Eq. 33:

(1) Inertial energy is negligible.
(2) Wicks are made up of spherical beads.

We have also made the assumption of neglecting gravity effects, but since the gravity can be included through Darcy's law, it is not listed above. Comparison of Eq. 33 with Eq. 21 gives the relation between the suction and capillary pressures as

$$p_s = \left(\frac{3}{2}\right)\left(\frac{R_p}{R_e}\right)\left(\frac{1-\varepsilon}{\varepsilon}\right)p_c \tag{35}$$

Here the capillary pressure p_c, which acts solely inside the hypothetical capillary tubes, is moderated by a function of porosity ε (with $0 < \varepsilon < 1$), mean pore size R_p, and effective bead radius R_e. For our assumption of spherical shape for beads, it turns out that $R_e > R_p$ (Table 3), and hence $p_s < p_c$. It is important to mention that if we assume the wicks to be a bundle of vertically aligned capillary tubes, we can still derive the expression for capillary pressure given in Eq. 21 using the same approach as used for obtaining Eq. 33. Substitution of p_s from Eq. 33 into Eqs. 18 and 19 allows us to

Table 1. Equations for the Height of Liquid Front h_f as Predicted by Different Models

Name of Model	Equation
Washburn equation	$h_f = \left(\frac{R_p \gamma \cos(\theta)}{4\tau^2 \mu}\right)^{1/2} \sqrt{t}$
Capillary model	$h_f = \sqrt{\frac{4K\gamma\cos(\theta)}{\varepsilon\mu R_p}}\sqrt{t}$
Capillary model with gravity	$p_c \ln\left\lvert\frac{p_c}{p_c-\rho g h_f}\right\rvert - \rho g h_f = \frac{\rho^2 g^2 K}{\varepsilon\mu} t,\ p_c = \frac{2\gamma\cos(\theta)}{R_p}$
EB model	$h_f = \sqrt{\frac{6K(1-\varepsilon)\gamma\cos(\theta)}{\varepsilon^2\ \mu R_e}}\sqrt{t}$
EB model with gravity	$p_s \ln\left\lvert\frac{p_s}{p_s-\rho g h_f}\right\rvert - \rho g h_f = \frac{\rho^2 g^2 K}{\varepsilon\mu} t,\ p_s = \frac{3(1-\varepsilon)\gamma\cos(\theta)}{\varepsilon R_e}$

derive expressions for liquid height h_f for the polymer wicks. The resulting equations, along with the corresponding equations for the capillary model, are summarized in Table 1.

Experimental Procedure

To study the wicking process through the commercial polymer wicks experimentally, some parameters about the wicks, the liquids, or the interaction between wicks and liquids should be found carefully. These parameters are: wick porosity (ε), wick permeability (K), mean pore radius (R_p), mean bead radius (R_b), liquid surface tension (γ), and dynamic contact angle (θ). The experimental techniques and results obtained for the testing materials are described briefly in this section.

Different bead sizes in the wicks lead to different permeability and pore sizes in them. These kinds of wicks, made by sintering polymer beads, are often used for delivering active liquids such as fragrances and insecticides from a reservoir to ambient air or other regions of interest. The most important polymers used for making wicks are polycarbonate (PC), polyethylene (PE), polypropylene (PP), and ethylene vinyl acetate. Among these, the first three are the most commonly used and are hence chosen for this study. We also used three different well-characterized alkane hydrocarbon liquids in the forms of hexadecane (HDEC), decane (DEC), and dodecane (DDEC) to see how variations in the liquid characteristics affect the wicking results. Alkane hydrocarbons are often the main solvents used for making insecticides/insect repellents by the consumer product companies; such solutions are released to the atmosphere through polymer wicks. Another reason for choosing the above alkane hydrocarbons as our test liquids was their low surface energies in comparison to the surface energies of chosen polymers, which cause their imbibition into the wicks to be spontaneous. (Due to the low surface energy of the polymers, these tests cannot be done with liquids of high surface energy such as water. PC, PE, and PP wicks are known to be hydrophobic as their contact angle with water is greater than 90°.) The characteristics of the liquids and wicks used in our experiments are presented in Tables 2 and 3.

We used a dynamic contact-angle analyzer (DCA) equipped with a sensitive balance with the accuracy of 0.0001 g to measure the absorbed mass in the wicks. The DCA has the capability of recording the weight of the wicks versus time; so with its special software we were enable to measure the wicking rates as well as the surface tension of the liquids and contact angles. The details of the experiments are described in the next few subsections.

Porosity

In this experiment, we used Gravimetric Test Method to find the mean porosity of wicks which is based on measuring the wicking rate. A DCA was used to accurately record the mass as a function of time, and the amount of liquid absorbed by the wicks is plotted against time. This curve has a positive slope but this slope decreases with time and reaches zero at full saturation. Since all pores of the wetted wick are filled with the liquid at the final saturation stage, the mean porosity (ε) of the cylindrical wick can be determined by the equation

$$\varepsilon = \frac{m_{sat}}{\rho\pi R_w^2 h_{f,ss}} \tag{36}$$

Note that $h_{f,ss} = L_w$ if the liquid traverses the complete wick length.

Permeability

Falling head permeameter (FHP) is a simple and effective technique for measuring the permeability of porous materials such as wicks.[28] A photo and a schematic of our testing setup are presented in Figure 3. A syringe is filled with a hydrocarbon liquid of known density and viscosity, and the wick is attached to the output end of the syringe. The setup is held vertically to enable the gravity force the liquid down the wick. The permeability of the wick is measured by measuring the liquid flow-rate in terms of the speed with which the liquid level goes down in the syringe. Later a formula derived from Darcy's law is used to calculate the permeability of the wick. This technique does not use a high applied pressure and so does not lead to wick compaction (and hence to an alteration in the distribution of the porosity and pore size in the wick), so it is suitable for quantifying the pore size and permeability of the wicks, especially for compressible wicks which could deform under high pressure. To get accurate results from this test, it was ensured that the test liquid did not flow over the sides of the wick by covering the wick surface with scotch tape completely.

Analysis presented here to estimate the permeability is almost identical to the derivation presented in section "Darcy's law-based wicking formulation" for wicking. However, there is an important difference between the two: the current analysis is for the fully saturated flow in the wick, whereas the earlier analysis is for the flow behind a rising front which is *assumed* to be fully saturated. As shown in Figure 3, a liquid-column of depth x in the syringe applies the hydrostatic pressure at the bottom to force the liquid through the wick of length L_w. Darcy's law applied to the saturated wick is

Table 2. Properties of the Test Liquids

Type of Liquid	HDEC	DEC	DDEC
Density, kg/m^3	773	730	750
Viscosity, mPa s	3.34	0.92	1.43
Surface tension, mJ/m^2	27.47	23.83	25.35

Refs. 29–31.

Table 3. Characteristics of the Test Wicks

Type of Wicks	A	B	C
Material	PC	PE	PP
Length of wick L, m	0.076	0.075	0.075
Wick radius R_w, m	0.0036	0.0036	0.0036
Pore radius R_p, μm	29.8 ± 7.1	36.7 ± 2.5	88.4 ± 4.4
Porosity, ε	0.49	0.41	0.4
Average bead radius R_b, μm	85.9 ± 9.9	133.1 ± 19.9	376.4 ± 30.1
Effective bead radius R_e, μm	97.9	164.1	428.5
Tortuosity, τ	2.38 ± 0.72	2.22 ± 0.81	1.58 ± 0.07
Permeability K, m^2	(5.46 ± 2.3)e − 11	(6.84 ± 1.16)e − 11	(3.9 ± 0.4)e − 10

R_p, R_b, τ, and K are presented with the 95% confidence interval range.[32]

$$V = -\frac{K}{\mu}\frac{dP}{d\xi} \tag{37}$$

where ξ is an upwardly oriented coordinate axis for the wick (Figure 3). This combined with the equation of continuity $\frac{dV}{d\xi} = 0$ yields $\frac{d^2P}{d\xi^2} = 0$ where $P = p + \rho g\xi$. Therefore, pressure distribution inside the wick is to be given by $P(\xi) = A\xi + B$ where A and B are determined from the boundary conditions

$$P = p_{atm} \text{ at } \xi = 0 \tag{38a}$$

$$P = p_{atm} + \rho g x \text{ at } \xi = L_w \tag{38b}$$

This results in

$$P(\xi) = \frac{\rho g x}{L_w}\xi + p_{atm} \tag{39}$$

as the pressure distribution inside the wick. Use of this equation in the Darcy's law (Eq. 37) yields

$$V = -\frac{K}{\mu}\frac{\rho g x}{L_w} \tag{40}$$

The flow rate in the wick is related to the magnitude of wicking velocity $|V|$ through the relation

$$Q = \varepsilon|V|\pi R_w^2 \tag{41}$$

Through the mass conservation principle, the flow rate is also related to the rate of depletion of liquid in the syringe as

$$Q = -\frac{dx}{dt}\pi R_s^2 \tag{42}$$

where x is the height of the liquid. By multiplying Eq. 40 by $\varepsilon\pi R_w^2$ and using it with Eqs. 41 and 42, the following equation is derived

$$\frac{dx}{dt} = -\frac{K\rho g R_w^2}{\mu L_w R_s^2}x \tag{43}$$

On separating the variables and integrating it, we get

$$\ln\left(\frac{x_0}{x}\right) = \frac{K\rho g R_w^2}{\mu L_w R_s^2}t \tag{44}$$

The initial condition of $x = x_0$ at $t = 0$ was applied in the integration. In a plot of $\ln\left(\frac{x_0}{x}\right)$ versus time, the slope of the trend line is equal to $\frac{K\rho g R_w^2}{\mu L_w R_s^2}$. Since all the other parameters in the "slope" equation are known, the permeability K can be found. Each test was repeated four times to make sure that the slope of the line had a repeatable value. The trend line and its slope for wick A (PC) is presented in Figure 4; and the test results are given in Table 3.

Mean pore radius of wicks

The mean pore size of the wick, to be used with the capillary model, can be estimated by the same device that is used for measuring the permeability. We once again assume the wick to consist of parallel capillary tubes. By applying the Hagen–Poiseuille law, the flow rate Q through the wick can be described by

$$Q = N\frac{\pi\rho g R_p^4(x + L_w)}{8\mu L_w} \tag{45}$$

After substituting Eq. 42 into Eq. 45, and integrating with the initial condition of $x = x_0$ at $t = 0$, the following equation is derived

$$\ln\left(\frac{x + L_w}{x_0 + L_w}\right) = -\frac{N\rho g R_p^4}{8R_s^2\mu L_w}t \tag{46}$$

Since N is the number of capillary tubes passing through the wick, so

$$N = \frac{\varepsilon\pi R_w^2}{\pi R_p^2} \tag{47}$$

Substitution of Eq. 47 into Eq. 46 leads to

$$\ln\left(\frac{x_0 + L_w}{x + L_w}\right) = \frac{\varepsilon R_w^2 R_p^2 \rho g}{8\mu L_w R_s^2}t \tag{48}$$

So by measuring the height of the fluid level, x, at various times and plotting $\ln\left(\frac{x+L_w}{x_0+L_w}\right)$ versus time, the slope of the trend line can be measured and pore radius R_p can be computed from Eq. 48. The measured pore radii for the three testing wicks are listed in Table 3.

Surface tension and contact angle

The standard Wilhelmy plate method was used in a DCA to measure the surface tension of the three test liquids. DCA

(a)

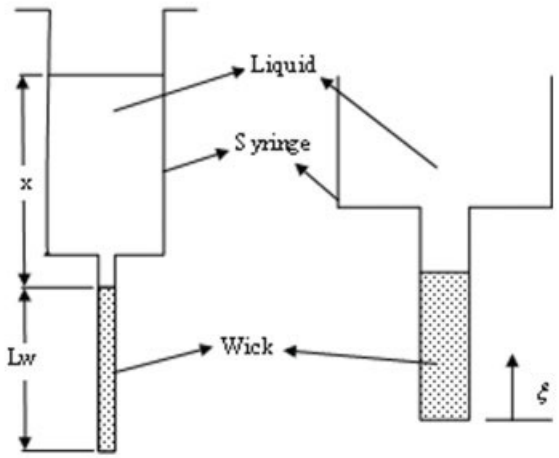

(b)

Figure 3. A photo and schematic of the FHP used for measuring the permeability and mean pore radius of the polymer wicks.

[Color figure can be viewed in the online issue, which is available at www.interscience.wiley.com.]

was also used to measure the dynamic contact angles of the wicks and liquids system. This new approach is based on the Washburn theory. According to Eqs. 1 and 20, the absorbed liquid mass into the pores of the wick obeys the relationship

$$m = \varepsilon\rho\pi R_w^2 \left(\frac{R_h\gamma\cos(\theta)}{2\tau^2\mu}\right)^{1/2}\sqrt{t} \tag{49}$$

Raising both sides to the power of two results in

$$m^2 = \frac{\lambda\rho^2\gamma\cos(\theta)}{\mu}t \tag{50}$$

where λ, the material constant, is equal to

$$\lambda = \frac{\varepsilon^2\pi^2 R_w^4 R_h}{2\tau^2} \tag{51}$$

The experiments were performed and the mass of the absorbed liquid was measured versus time. The setup shown in Figure 2 was used to estimate the contact angles through this Washburn-theory based approach. A plot of m^2 versus t was used to find the slope of the best fitted line; this slope in turn was used to find the constant λ and contact angle for the testing wick. First, the experiments were performed with a liquid in which the contact angle is close to zero, so that we could use the slope of the best fitted line to estimate λ. For this reason we used *N*-hexane, a liquid with a very low surface tension. It was then possible to perform the same experiments with the three test liquids, and estimate the contact angle for liquids and the wick through the use of Eq. 50.

This newly proposed method is valid when λ can be assumed to remain constant for a given wick from one experiment to the next. According to Eq. 46, the material constant λ is a geometry based term that is a function of the macro-geometric parameters (such as R_w) and the micro-geometric parameters (such as ε, R_h, and τ). Because λ was assumed to be constant, we ensured that each wick sample has the same size, shape, and pore orientation during these experiments.

Incidentally, the measured contact angles were found to be zero for all combinations of the considered testing liquids and wicks. This was to be expected since the surface energy of wicks was much higher than that of the liquids.

Tortuosity

The micrographs of the wicks were used to estimate the tortuosity of the porous medium. Figure 1 shows two microscopic cross-sections of the wick C (PP) along and across its length, and shows our method to measure the tortuosity.

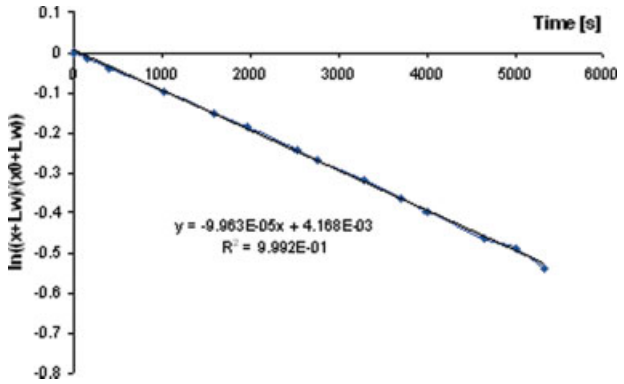

Figure 4. The experimental plot used for estimating the mean pore radius in wick A (PC).

[Color figure can be viewed in the online issue, which is available at www.interscience.wiley.com.]

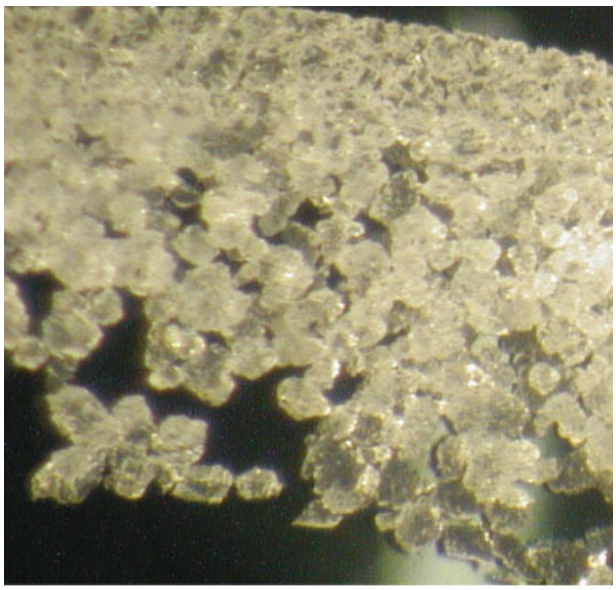

(a)

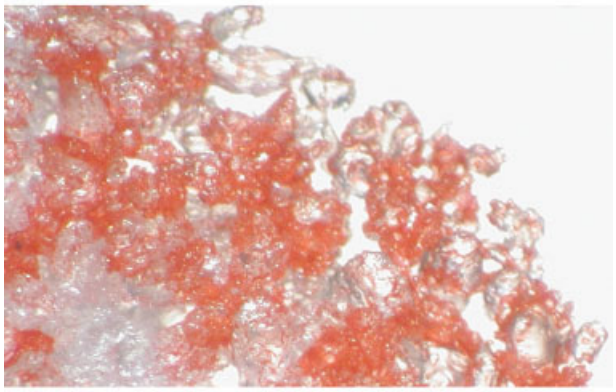

(b)

Figure 5. Micrographs of wicks A (PC) and B (PE) showing the shape and size variations in the individual beads.

(a) Wick A; (b) wick B. [Color figure can be viewed in the online issue, which is available at www.interscience.wiley.com.]

Three pairs of points across the wick and another three pairs along the wick were considered to measure the mean tortuosity for each wick. The measured tortuosities, listed in Table 3, enabled us to use the modified Washburn equation, Eq. 6.

(Incidentally, if we consider an idealized spherical geometry for polymer beads that constitute the wicks, the ratio of L_e/L will be equal to $\frac{\pi}{2}$ for a path wrapped around an individual bead, as it is the ratio of half of the circular section perimeter to its diameter. The resultant tortuosity τ obtained from Eq. 2 is 2.47, which is of the same order-of-magnitude as the values listed in Table 3.)

Effective bead radius

The micrographs of the wicks were also used to measure the bead size distribution and to observe the range of variations in bead shapes for different wicks (Figures 1 and 5). The frequency distribution of the measured bead radii was presented in the form of a histogram for all the three wicks. (The histogram for wick C (PP) is shown in Figure 6.) As described under Eq. 31, the effective radius should be estimated as

$$R_e = \frac{M_3}{M_2} = \frac{\int_0^\infty r^3 \phi(r) dr}{\int_0^\infty r^2 \phi(r) dr} \tag{52}$$

Since discrete frequencies are plotted in the histogram, so the corresponding discrete *probability density function* for each bead radius R_{b_i} can be determined by

$$\phi(R_{b_i}) = \frac{\text{frequency corresponding to } R_{b_i}}{T} \tag{53}$$

where T is the sum of all frequencies. The discrete form of Eq. 52 is

$$R_e = \frac{\sum_{R_b,\min}^{R_b,\max} {R_{b_i}}^3 \phi(R_{b_i})}{\sum_{R_b,\min}^{R_b,\max} {R_{b_i}}^2 \phi(R_{b_i})} \tag{54}$$

where the effective radius R_e can be obtained after using the ϕ estimated through Eq. 53. The measured effective and mean bead radii for the considered wicks are presented in Table 3.

Results and Discussion

To predict the absorbed mass into the wicks, we used the following five models and compared their predictions with the experimental results. Nomenclatures corresponding to the five models, details of which are listed in Table 1, are as follows:

(1) The modified Washburn model, Eq. 6, would be named "Washburn Model."

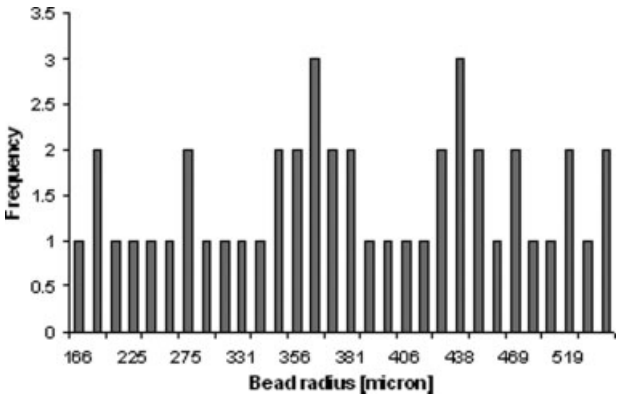

Figure 6. Frequency distribution corresponding to bead radius for wick C (PP).

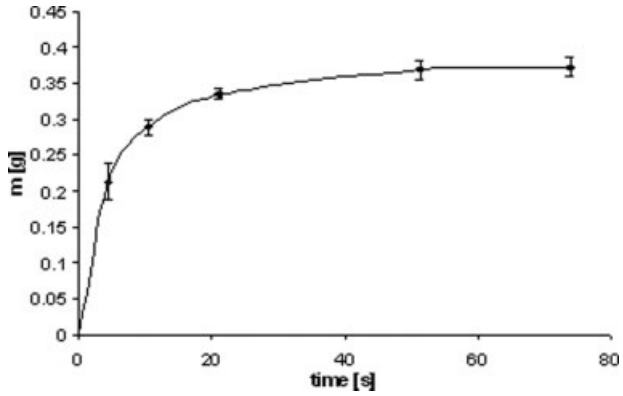

Figure 7. Scattering test on wick C (PP) with HDEC.

Scatter bars show confidence interval of 95%.

(2) The capillary model without the gravity effect would be named "Capillary Model."

(3) The capillary model including the gravity effect would be named "Capillary Model with gravity."

(4) The EB model without the gravity effect would be named "EB Model."

(5) The EB model including the gravity effect would be named "EB Model with gravity."

As we mentioned before, we used three different polymer wicks with three different mean pore and effective bead radii. In the wicks A (PC) and B (PE) the pore radii are small enough such that the suction pressure can saturate all the lengths of the wick (length 0.074 m) after touching the liquid from one end of the wick. In the wick C (PP), the pore size is very large such that the suction pressure is not strong enough to saturate the wick completely. In this case, the liquid rises to a height that is less than the wick length and the downward pull due to gravity is equal to the upward pull of the suction pressure at this stage; the absorption stops at this point. It was noticed that around this stationary point, a little below and above this front position, the wick saturation was not complete or 100%. Over a certain length, the saturation was visually observed to gradually decrease from 100% before the front to 0% at slightly ahead of the front. Since all the above-mentioned models are based on the assumption of complete saturation behind the front liquid, the presence of partial saturation near the front may contribute to some extent to the observed differences between the model predictions and the experimental observations.

We did a scatter-estimation test on the wick C (PP) to estimate the repeatability of the test results. Figure 7 shows the results of scatter-estimation tests on wick C (PP) with HDEC; the measured 95% confidence intervals[32] are shown with the help of scatter bars. (This interval is a range of the measured quantity in which the measured value is expected to fall 95% of the times.) The smallness of these bars means that our experiments were very repeatable. We are confident that all experiments listed in this article show similar repeatability patterns. One reason for this excellent repeatability could be the extremely consistent pore structure of the commercial polymer wicks chosen for this experiment.

Similarly, tests to measure various properties (Table 3) were often conducted multiple times to obtain more than one measured values. The scatter in the property values thus obtained was quantified through the use of the 95% confidence interval.[32]

Note that the micrographs of the wicks were used to get a visual estimation for porosity and mean pore size to corroborate what we measured using the tests described in sections "Porosity (ε)" and Mean pore radius of wicks (R_p). The porosity was measured by dividing the pore area within an arbitrary rectangle by the total rectangle area. A typical pore size was estimated from the radius of the largest circle that can be fitted between the polymer beads. The porosity and mean pore size estimated through the two different methods were found to be quite close. As described in previous sections, the micrographs also were used to measure the tortuosity and bead sizes.

Wicking tests and comparison with the predictions of various models

The results of wicking tests and the predictions for wick A (PC) are shown in Figure 8. As per the plots, the "EB Model with gravity" performs better than the other models. As the time increases, all predictions diverge away from the experimental results. Comparison of parts a–c of Figure 8 indicates that as the viscosity of the test liquid reduces (Table 2), the difference between the "EB Model with gravity" prediction and the experimental results also reduces. It is also to be noted that the liquid mass absorbed by wick A (PC) is the highest for the least viscous liquid, DEC.

Figure 9 shows the test results and predictions for Wick B (PE). Again the "EB Model with gravity" performs better than the capillary models; surprisingly, predictions of the "Washburn Model" are perhaps equally good. The former, though inaccurate in the beginning of the wicking process, becomes more accurate with time. The latter, though more accurate in the beginning, progressively loses its accuracy with time. It is clear that the predictions of the capillary model, even after including the gravity effect, do not compare well with the experimental observations.

Figure 10 shows the predictions of various models and experimental observations for the wick C (PP). As described before, due to its large pore size, this wick could not be completely saturated along all of its length as the suction pressure at liquid front is not strong enough to raise the liquids to the top of the wick. Due to this effect, this is a good wick to test the predictions for the maximum absorbed mass under steady state condition. As shown in the figures, none of the models, except the newly proposed "EB Model with gravity" can predict the maximum mass absorbed in the wick. Since the absorbed mass in a wick is proportional to the height to which a liquid rises, the final steady-state height reached by the three liquids in this PP wick is only predicted by the "EB Model with gravity." This heartening observation establishes that it might be the most accurate of all the models considered in this study.

(Incidentally our Darcy-based approach allows us to compute steady-state height* as $h_{f,ss} = p_s / \rho g$ for EB model with gravity, and $h_{f,ss} = p_c / \rho g$ for capillary model with gravity. As is clear from Eq. 35, $p_s < p_c$ and hence $h_{f,ss}$ for

*The steady-state fluid-column height in a wick is obtained by noting that dh_f/dt in Eq. 17 is equal to zero at the final state.

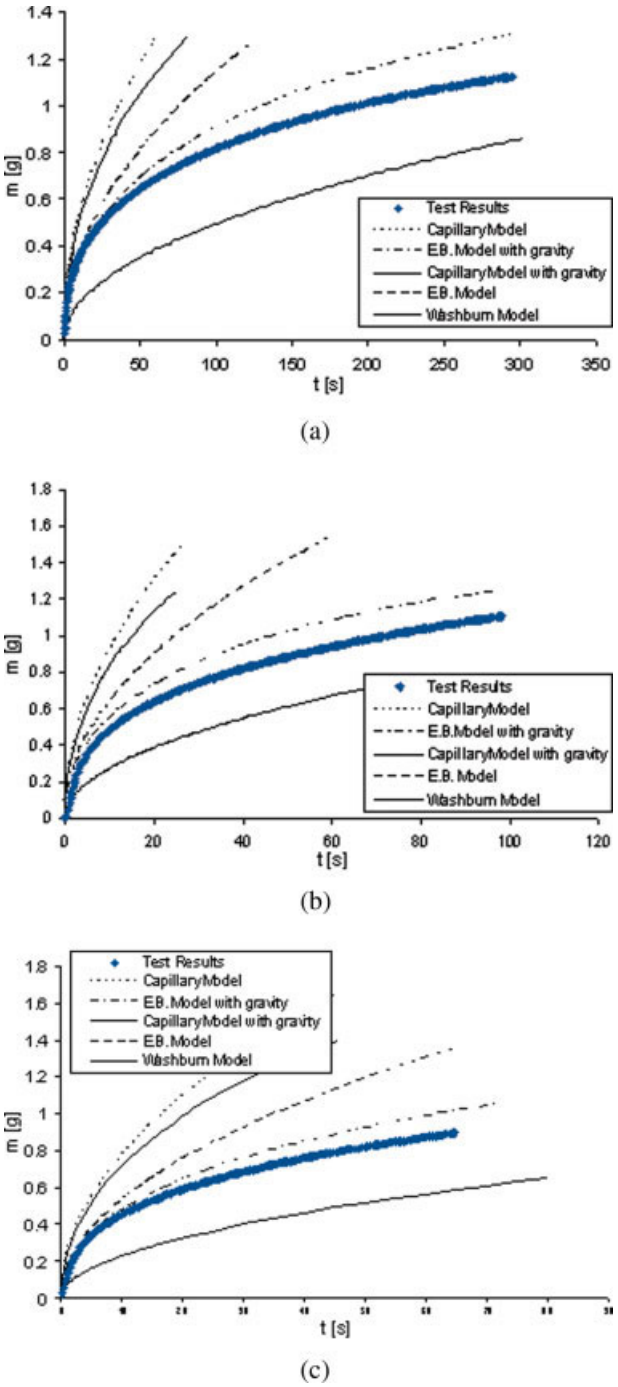

Figure 8. Mass absorption rate in wick A (PC) with three different liquids.

(a) With HDEC; (b) with DEC; (c) with DDEC. [Color figure can be viewed in the online issue, which is available at www.interscience.wiley.com.]

the EB model is smaller than that for the capillary model. The steady-state mass in wick C (Figure 10) that is thus obtained from $h_{f,ss}$ can be shown to be very close to the large-time asymptotic value predicted by the EB model with gravity.)

A possible reason for the difference between the experimental results and the predictions of newly proposed EB model with gravity is the deviation of bead shapes from assumed spherical shape. Most beads in wick B have non-spherical irregular shapes, and that perhaps explains the difference between the experimental results and theoretical predictions of the EB model with gravity in Figure 9. A strong agreement of the model with experiment for wick C (Figure 10)

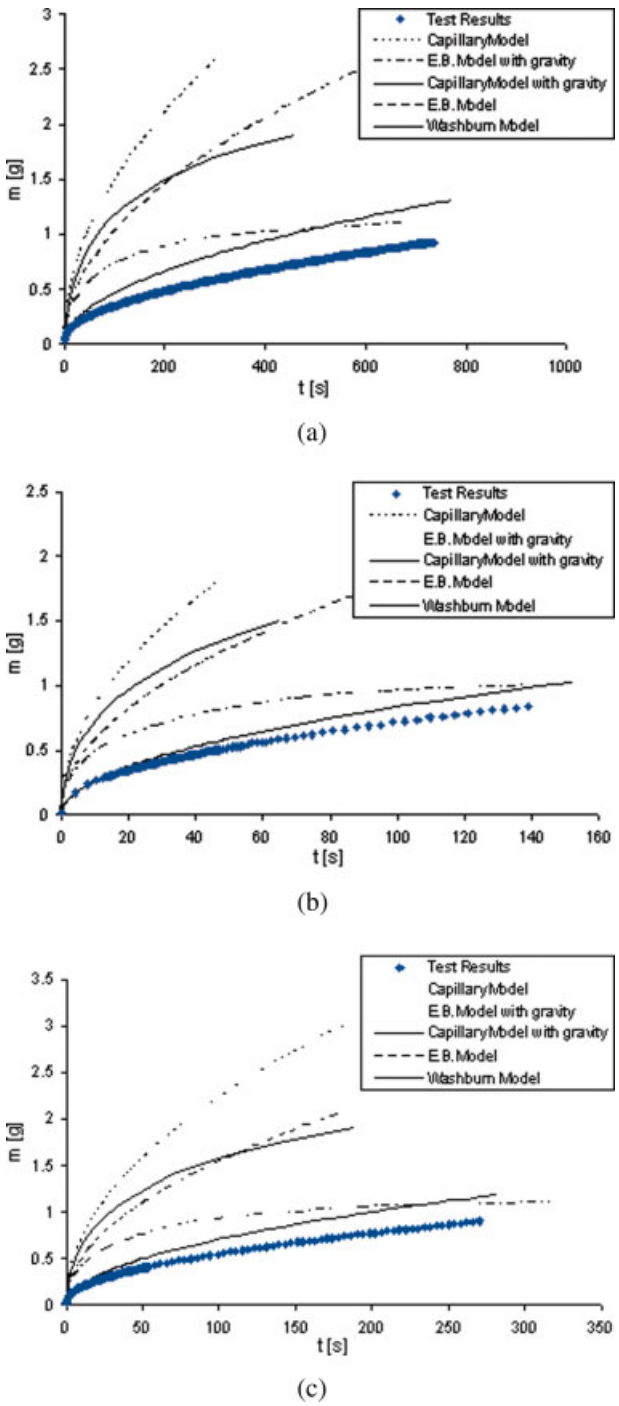

Figure 9. Mass absorption rate in wick B (PE) with three different liquids.

(a) With HDEC; (b) with DEC; (c) with DDEC. [Color figure can be viewed in the online issue, which is available at www.interscience.wiley.com.]

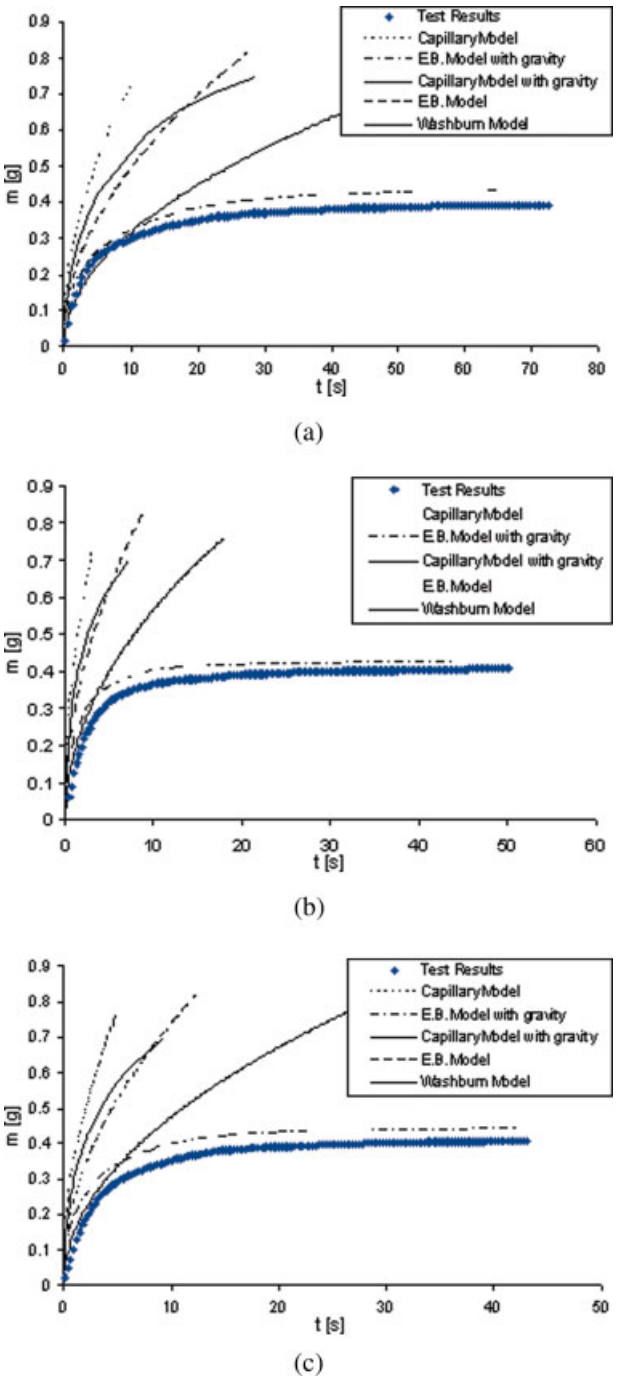

Figure 10. Mass absorption rate in wick C (PP) with three different liquids.

(a) With HDEC; (b) with DEC; (c) with DDEC. [Color figure can be viewed in the online issue, which is available at www.interscience.wiley.com.]

may have something to do with the almost spherical shape of its beads shown in Figure 1.

As the only difference between the EB and capillary models is in the expression for the suction pressure, so this prediction indicates that the newly proposed suction-pressure expression works better than one applied with the conventional models for such polymer wicks. The reason could be the inclusion of porosity ε, effective bead radius R_e, and mean pore radius R_p, the three additional parameters related to the microstructural attributes of the wick, in the definition of the suction pressure in the EB models (Eq. 35). We anticipate that adding of more parameters related to wick microstructure, such as the bead shape distribution, in the suction-pressure expression will probably improve the prediction even more.

From the study of Figures 8–10, it is clear that both the EB as well as the capillary models have a tendency to grossly over-predict the mass absorption rate. However, they improve their predictions after inclusion of the gravity effects. So gravity cannot be neglected for our system of 7.5-cm long PC, PE, PP wicks and the alkane hydrocarbon liquids HDEC, DEC, and DDEC.

From the present experimental study, it is also clear that the capillary models are perhaps the worst of all the models considered, and an explanation of the failure of these models is in order here. In the polymer wicks made of small beads with irregular shapes and sizes, the capillary tube assumption of having a bundle of aligned fixed-diameter tubes is clearly not satisfied—the size and shape of the pores vary along any flow direction, and might even be different along and across the wick (Figure 1). Moreover, numerous interconnections exist between the pores. So the capillary model can perhaps be improved if the effect of the shape and size variations in pores along with the inter-pore interconnections is somehow included in the definition of the suction pressure.

Summary and Conclusion

We use the Darcy's law to model the absorption of a liquid into a wick made from sintering polymer beads. A new expression for suction pressure at the liquid front inside the wick is formulated based on the balance of surface energy and viscous dissipation energy; such an expression is found to depend on both the mean bead size and the porosity of the wick. Another expression for suction pressure, which treats the porous wick as a bundle of capillary tubes, is also formulated. These two different expressions for the suction pressure, when implemented with the Darcy's law based formulation, lead to two different flow models: one the EB model, and the other the capillary model. Two further variants of these models were considered after incorporating the effect of gravity.

As a case study of these wicking models, a set of tests using three different polymer wicks (PC, PE, and PP) and three different hydrocarbon liquids (HDEC, DEC, and DDEC) were conducted. In these tests, the mass absorbed through wicking is plotted as a function of time while all parameters used in the proposed model were measured accurately and no fitting parameters were used. The traditional Washburn's equation was also employed to predict the mass gain during wicking. Of all the different models used, the newly proposed EB method in conjunction with gravity yields the most satisfying predictions. The success of this method is especially notable for a large-pore PP wick where it was the only model to predict the final steady-state height of the liquid column.

This work is characterized with several novel features. The main original contribution is in the development of a new expression for suction pressure in polymer wicks based on the EB principle. The other important contribution is in the form of some new techniques that have been used to estimate the property parameters in the wicking models. For example, measurement of the wick permeability with the FHP is a novelty to the science of wicking. Similarly, the use of wick micrographs to estimate parameters such as the porosity, the tortuosity, and the effective bead radius (through the use of histogram of bead size distribution), is new to the field of wicking studies. We have also proposed a new method to estimate the contact angle of wicking liquids inside the wicks. As a result of the independent estimation of various model parameters, the proposed EB model with gravity model predicts the experimental results rather well *without the use of any fitting parameters*.

Acknowledgments

The authors are grateful to Dr. Andrei Skliarov and Dr. Steve Hardcastle for their help in micrography, and Dr. Marjorie Piechowski for her help in editing.

Notation

A_{cs} = cross-sectional area of the wick
dA = a differential amount of the interfacial (solid-pore) wetted area
d_p = mean pore diameter
F_p = pulling force
g = acceleration due to gravity
h = height coordinate in the wetted wick (Figure 3)
h_f = height of the liquid front in the wick (Figure 3)
$h_{f,ss}$ = final steady-state height of the liquid front in the wick
K = permeability of the wick
L = the straight-line distance between two arbitrary points in the wick (Figure 4)
L_e = effective length of the path in which the liquid moves between two points (Figure 4)
L_w = wick length
M = total number of the beads in the wick
M_2 = second moment of the bead-size distribution, Eq. 29
M_3 = third moment of the bead-size distribution, Eq. 27
m = absorbed liquid mass
m_{sat} = mass of liquid in fully saturated wick
M_v = viscose work
N = number of capillaries passing along the wick
p = pore averaged liquid pressure
P = pore averaged modified pressure
p_c = capillary pressure
p_s = suction pressure
p_{atm} = atmospheric pressure
Q = mass flow rate
R_h = hydraulic radius
R_p = mean pore radius
R_b = mean bead radius
$R_{b,max}$ = maximum bead radius in a section of the wick
$R_{b,max}$ = minimum bead radius in a section of the wick
R_e = effective bead radius
R_w = wick radius
R_s = reservoir internal radius
T = sum of all frequencies in a bead-size distribution histogram
t = time
V = Darcy's velocity
V_b = total bead volume in the wick
V_t = total volume of the wick
W_v = viscous dissipation energy
W_m = mechanical work
x = liquid height in the reservoir at t
x_0 = liquid height in the reservoir at $t = 0$
λ = the material constant in Washburn equation
ε = porosity of the wick
ρ = density of the liquid
γ = surface tension of the liquid
γ_s = surface energy in dry surface
γ_{sl} = surface energy in wetted surface
θ = contact angle
τ = tortuosity of the wick
ϕ = probability density function for bead-size distribution in polymer wicks
μ = viscosity of the liquid

Literature Cited

1. Lucas R. Rate of capillary ascension of liquids. *Kollid Z.* 1918;23:15.
2. EV Washburn. The dynamics of capillary flow. *Phys Rev.* 1921; 17:273.
3. Sutera, SP. The history of Poiseuille's law. *Annu Rev Fluid Mech.* 1993;25:1–19.
4. Chatterjee PK. *Absorbency*. Amsterdam: Elsevier, 1985.
5. Szekely J, Neumann AW, Chuang YK. The rate of capillary penetration and the applicability of the Washburn equation. *J Colloid Interface Sci.* 1971;35:273–278.
6. Chwastiak S. A wicking method for measuring wetting properties of carbon yarn. *J Colloid Interface Sci.* 1973;42:298–309.
7. Scher KE. Master's Thesis. Department of Chemical Engineering. University of Washington, 1983.
8. Hodgson KT, Berg JC. The effect of surfactants on wicking flow in fiber networks. *J Colloid Interface Sci.* 1988;121:22–31.
9. Fowkes FM. Role of surface active agents in wetting. *J Phys Chem.* 1953;57:98–103.
10. Williams JG, Morris CE, Ennis BC. Liquid flow through aligned fiber beds. *Polym Eng Sci.* 1979;14:413–419.
11. Pillai KM, Advani SG. Wicking across a fiber-bank. *J Colloid Interface Sci.* 1996;183:100–110.
12. Young T. An essay on the cohesion of fluids. *Philos Trans R Soc Lond.* 1805;95:65–87.
13. Gauss K. *Gott Gelehrte Anz.* 1829;1641.
14. Dussan V, Davis SH. On the motion of a fluid–solid interface along a solid surface. *J Fluid Mech.* 1974;65:71–95.
15. Dussan V. On the spreading of liquids on solid surfaces: static and dynamic contact lines. *Annu Rev Fluid Mech.* 1979;11:371–400.
16. Hsieh Y-L. Novel surface chemistry and geometric features of fibers: regulation of liquid wetting and absorption. INTC International Nonwovens Technical Conference, Millennium Hotel, Sept. 2005:19–22.
17. BS 3424 Method 21. British Standard, 1973.
18. DIN 53924. German Standard, 1978.
19. Kissa E. Wetting and wicking. *Text Res J.* 1996;66:660–668.
20. Miller B. Critical evaluation of upward wicking tests. *Int Nonwoven J.* 2000;9:79–87.
21. Russell SJ, Mao N. Apparatus and method for assessment of in-plane anisotropic liquid absorption in nonwoven fabrics. *AUTEX Res J.* 2000;1:47–53.
22. Jeong JK. Slip boundary condition on an idealized porous wall. *Phys Fluids.* 2001;13:1884–1890.
23. Mao N, Russell SJ. Prediction of liquid absorption in homogeneous three dimensional nonwoven structures. International Nonwoven Technical Conference, Atlanta, 2002.
24. Mao N, Russell SJ. Anisotropic liquid absorption in homogeneous two dimensional nonwoven structures. *J Appl Phys.* 2003;94:4135–4138.
25. Lockington DA, Parlange JY. Anomalous water absorption in porous materials. *J Phys D: Appl Phys.* 2003;36:760–767.
26. Gane PAC, Ridgway CJ, Schoelkopf J. Absorption rate and volume dependency on the complexity of porous network structures. *Transp Porous Media.* 2004;54:79–106.

27. Tucker CL, Dessenberger RB. Governing equation for flow and heat transfer in stationary fiber beds. In: Advani SG, editor. *Flow and Rheology in Polymer Composites Manufacturing*. Amsterdam: Elsevier, 1994, Chapter 8.
28. Bear J. *Dynamics of Fluids in Porous Media*. New York: Elsevier, 1972.
29. Material Database. In: Sigma 701 Tentiometer, KSV Instruments Ltd.
30. Caudell DR, Trusler JPM, Vesovie V, Wakeham WA. The viscosity and density of *n*-dodecane and *n*-octadecane at pressure up to 200 mPa and temperatures up to 473 K. Available at http://symp15.nist.gov/pdf/p175.pdf.
31. Wikipedia. The free encyclopedia. Available at http://en.wikipedia.org/wiki/Decane.
32. Wheeler AJ, Ganji AR. *Introduction to Engineering Experimentation*. Upper Saddle River, NJ: Prentice Hall, 1996.

Manuscript received Apr. 20, 2007, and revision received July 27, 2007.